

Growth of persistent foci of DNA damage checkpoint factors is essential for
amplification of G1 checkpoint signaling

Motohiro Yamauchi^{1*}, Yasuyoshi Oka¹, Masashi Yamamoto², Koichi Niimura²,
Motoyuki Uchida², Seiji Kodama³, Masami Watanabe⁴, Ichiro Sekine¹,
Shunichi Yamashita¹, Keiji Suzuki¹

¹Atomic Bomb Disease Institute, Graduate School of Biomedical Sciences, Nagasaki
University, 1-12-4 Sakamoto, Nagasaki 852-8523, Japan

²Biomedical Research Laboratories, Kureha Corporation, 3-26-2 Hyakunincho,
Shinjyuku, Tokyo 169-8503, Japan

³Division of Radiation Biology and Health Science, Research Institute for Advanced
Science and Technology, Osaka Prefecture University, 1-2 Gakuen-cho, Sakai, Osaka
599-8570, Japan

⁴Laboratory of Radiation Biology, Research Reactor Institute, Kyoto University, 2-1010
Asashironishi, Kumatori-cho, Sennan-gun, Osaka 590-0494, Japan

*Corresponding author

Tel: +81-95-848-7116; Fax: +81-95-848-7117; E-mail: motoyama@nagasaki-u.ac.jp

Keywords

ATM, persistent foci, foci growth, signal amplification, G1 arrest

Abstract

Several DNA damage checkpoint factors form nuclear foci in response to ionizing radiation (IR). Although the number of the initial foci decreases concomitantly with DNA double-strand break repair, some fraction of foci persists. To date, the physiological role of the persistent foci has been poorly understood. Here we examined foci of Ser1981-phosphorylated ATM in normal human diploid cells exposed to 1 Gy of X-rays. While the initial foci size was approximately 0.6 μm , the one or two of persistent focus (foci) grew, whose diameter reached 1.6 μm or more in diameter at 24 h after IR. All of the grown persistent foci of phosphorylated ATM colocalized with the persistent foci of Ser139-phosphorylated histone H2AX, MDC1, 53BP1 and NBS1, which also grew similarly. When G0-synchronized normal human cells were released immediately after 1 Gy of X-rays and incubated for 24 h, the grown large phosphorylated ATM foci ($\geq 1.6 \mu\text{m}$) were rarely (av. 0.9%) observed in S phase cells, while smaller foci ($< 1.6 \mu\text{m}$) were frequently (av. 45.9%) found. We observed significant phosphorylation of p53 at Ser15 in cells with a single grown phosphorylated ATM focus. Furthermore, persistent inhibition of foci growth of phosphorylated ATM

by an ATM inhibitor, KU55933, completely abrogated p53 phosphorylation. Defective growth of the persistent IR-induced foci was observed in primary fibroblasts derived from ataxia-telangiectasia (AT) and Nijmegen breakage syndrome (NBS) patients, which were abnormal in IR-induced G1 checkpoint.

These results indicate that the growth of the persistent foci of the DNA damage checkpoint factors plays a pivotal role in G1 arrest, which amplifies G1 checkpoint signals sufficiently for phosphorylating p53 in cells with a limited number of remaining foci.

1. Introduction

Human cells have evolved highly sophisticated mechanisms of cell cycle checkpoint to counteract DNA damage caused by various environmental stresses, such as ionizing radiation (IR). The central player in cell cycle checkpoint is ATM protein kinase, which is a responsible gene product for cancer-predisposed disease, ataxia-telangiectasia (AT) [1]. Cells derived from AT patients show higher radiosensitivity, and have defects in DNA double-strand break (DSB) repair and IR-induced cell cycle checkpoints [2-5]. ATM belongs to phosphatidylinositol 3-kinase family, and it phosphorylates many checkpoint-, or repair-related proteins, including p53 (Ser15), CHK2/hCds1 (Thr68), and NBS1 (Ser278, and 343) [6-12]. Bakkenist and Kastan reported that ATM forms dimer or high-order multimer in unperturbed cells, and in response to IR, it is activated through intermolecular autophosphorylation at its Ser1981 and dimer dissociation [13]. Interestingly, these phosphorylated ATM molecules concentrate at specific sites in the nucleus after IR, which are visualized as “foci” by immunofluorescence staining [13]. One of the ATM substrates is histone

H2AX, which belongs to the core histone H2A subfamily [14, 15]. H2AX is phosphorylated by ATM at its C-terminal Ser139 in response to IR [15]. The phosphorylated H2AX also forms discrete foci in the nucleus after IR, and the foci colocalize with phosphorylated ATM foci [13, 16, 17]. The number of phosphorylated H2AX foci is well consistent with the theoretically calculated number of DSBs produced by IR, and the foci number decreases gradually after irradiation, reflecting DSB repair [16, 17]. Recent studies demonstrated that several other proteins also form foci in the nucleus after IR. For example, 53BP1, which was originally isolated as a p53-binding protein, forms foci in the nucleus after IR, and the 53BP1 foci colocalize with phosphorylated H2AX foci [18-20]. MDC1, which was isolated as a factor associated with MRE11-Rad50-NBS1 complex, also forms foci colocalized with phosphorylated H2AX foci after IR [21].

There is accumulating evidence that these focus-forming factors are involved in IR-induced checkpoint. Fernandez-Capetillo et al. reported that G2/M checkpoint is impaired in H2AX-, or 53BP1 knockout mouse after low doses (≤ 2 Gy) of IR [22]. It was also reported that radioresistant DNA synthesis (RDS) phenotype, which suggests

aberration of IR-induced S checkpoint, is observed in 53BP1-siRNA-expressing cells [23]. MDC1-knocked-down cells also show partial defect in S-, or G2/M checkpoint after IR [24, 25]. Substrate phosphorylation by ATM seems to occur at damaged site, because Lukas et al. demonstrated that Thr68 phosphorylation of CHK2-hCds1 occurs only at laser-microirradiated site, using ectopically-expressed CHK2 protein immobilized by fusion with histone H2B [26]. These results suggest that foci of phosphorylated H2AX, 53BP1, and MDC1 serve as molecular scaffolds of substrate phosphorylation by ATM.

As mentioned above, relationship between the initially-formed IR-induced foci and checkpoint activation has been intensively studied. However, the initial foci number decreases concurrently with DNA repair, and only a few foci persist for over 24 h, particularly with low doses of IR, such as 1 Gy. Because G1 checkpoint activation is slowly elicited, most of the initial foci disappear while G1 arrest persists. Thus, cells with a limited number of persistent foci should have a mechanism to amplify G1 checkpoint signals. Because the standard technique, such as western blotting, fails to detect changes in foci, we examined the role of the persistent foci of phosphorylated

ATM in individual cells by immunofluorescence staining. We found the persistent foci grew in size, and the foci growth is essential for G1 arrest. We propose that it is the persistent phosphorylated ATM foci, not the initial foci, that determine whether cells are arrested at G1/S border, and the growth of the persistent foci is the indispensable mechanism for amplification of G1 checkpoint signaling in cells with a limited number of foci.

2. Materials and methods

2.1. Cell culture and irradiation

Normal human diploid cells (HE49), primary fibroblasts derived from patients with ataxia telangiectasia (AT2KY and AT5BI) and Nijmegen breakage syndrome (WG1799) were cultured in minimal essential Eagle's media (MEM) containing 10% fetal bovine serum (ThermoTrace Ltd., Australia). Five to ten $\times 10^4$ cells were seeded onto 22 mm x 22 mm coverslips in 35 mm dishes. Two days later, cells were irradiated with X-rays from X-ray generator at 150 kVp and 5 mA with a 0.1 mm copper filter at a dose rate of 0.492 Gy/min. Nutlin-3 (Alexis biochemicals, USA) was dissolved in DMSO to prepare 8 mM stock solution, and was treated at a final concentration of 8, or 32 μ M. KU55933 was dissolved in DMSO to prepare 20 mM stock solution, and was treated at a final concentration of 10 μ M.

2.2. Synchronization of cell cycle

G0 synchronization was achieved by contact inhibition. One $\times 10^6$ of HE49 cells or WG1799 cells were plated in T25 flasks (25 cm²) and cultured 14 days (HE49) or 28 days (WG1799), with changing the culture media every 3 or 4 days. Under these conditions, less than 2% of cells showed staining of replication protein A and Ser10-phosphorylated histone H3, which indicate S phase cells and G2/M phase cells, respectively. At day 15 or 29, cells were irradiated, harvested with trypsin immediately after IR, and 1×10^5 cells were replated onto 22 x 22 mm coverslips in 35 mm dishes to release from synchronization. Thereafter, cells were fixed followed by immunofluorescence staining.

2.3. Immunofluorescence staining

For immunofluorescence staining, cells were once washed with 1 x PBS⁻, and were fixed with 4% formaldehyde in 1 x PBS⁻ for 10 min, then permeabilized with 0.5%

Triton X-100 in 1 x PBS⁻ for 5 min. For RPA staining, cells were once washed with CSK buffer (10 mM HEPES-KOH, pH 7.4, 300 mM Sucrose, 100 mM NaCl, 3 mM MgCl₂ · 6H₂O), then extracted with 0.5% Triton X-100 in 1 x PBS⁻ for 2 min. After extraction, cells were fixed with 4% formaldehyde in 1 x PBS⁻ for 20 min, and then, permeabilized with 0.5% Nonidet P-40 in 1 x PBS⁻ for 5 min. For bromodeoxyuridine (BrdU) staining, G₀-synchronized HE49 cells were treated with 0.5 mM BrdU/0.05 mM fluorodeoxyuridine (FIdU) immediately after release from synchronization, and cells were incubated in the media containing BrdU/FIdU until fixation. Twenty-four hours after release, cells were once washed by 1 x PBS⁻, then fixed with 100% methanol for 5 min. After fixation, cells were treated with 1 N HCl for 30 min, to hydrolyze DNA. All reagents were chilled, and all procedures were performed on ice. After permeabilization, primary antibody for phosphorylated ATM at Ser1981 (mouse; Rockland, USA, clone 10H11.E12, rabbit; Rockland, USA), phosphorylated histone H2AX at Ser139 (mouse; Upstate, USA, clone JBW301), MDC1 (rabbit; Bethyl, USA), 53BP1 (mouse; Calbiochem, USA, clone BP13, rabbit; Bethyl, USA), NBS1 (mouse; Genetex, USA, clone 1D7), 34 kDa subunit of replication protein A (RPA, mouse; Calbiochem, USA,

clone RPA34-19), BrdU (mouse; Roche Applied Science, Switzerland, clone BMC9318), phosphorylated histone H3 at Ser10 (mouse; Upstate, USA, clone RR002, rabbit; Upstate, USA), or phosphorylated p53 at Ser15 (rabbit; Cell Signaling Technology, USA) was treated for 2 h in a 37°C humidified CO₂ incubator. After washing with 1 x PBS⁻ for 3 times, secondary antibody conjugated with Alexa 488 or 594 (Molecular Probes, USA) was treated for 1 h in the incubator. All antibodies were dissolved in TBS-DT (20mM Tris-HCl, 137mM NaCl, 0.1% Tween 20, 125µg/ml ampicillin, 5% skim milk). After washing with 1 x PBS⁻ for 3 times, coverslips were mounted onto slide glasses with 10% Glycerol in 1 x PBS⁻. The digital images of the primary antibodies were acquired using fluorescence microscopy (DM6000B, Leica, Germany). Foci analysis was performed by using maximum intensity projection (MIP) images. The Z-plane stacks of images of foci were captured at 200-300 nm intervals, and 10-20 images at each focal plane were collected. Then, regions at maximum intensity at each focal plane were assembled into a 2D MIP image using FW4000 software (Leica, Germany). Focus diameter was measured using FW4000, by encircling the focus in the captured image. In the present study, we described the major axis of the

focus as “diameter”, because the focus of the proteins is not a *bona fide* circle. Fluorescence intensity of phosphorylated ATM and phosphorylated p53 was measured by the following procedure: the nucleus stained by DAPI was encircled and fluorescence intensity in the encircled area was measured. The area outside the nucleus was also encircled and fluorescence intensity in the area was measured to obtain background intensity. The intensity outside the nucleus was subtracted from the intensity in the nucleus to obtain actual nuclear intensity of the proteins.

3. Results

3.1. Growth of persistent IR-induced foci in normal human diploid cells

To know the dynamics of IR-induced foci, we first performed spatiotemporal analysis of Ser1981-phosphorylated ATM foci after 1 Gy of X-rays in normal human diploid cells (Fig. 1). While most of the unirradiated cells had no phosphorylated ATM foci, many tiny foci of phosphorylated ATM were detected immediately after IR. The initial foci number peaked at 15 min (av. 36.9 per nucleus), and decreased subsequently, reflecting DSB repair (Fig. 1A).

As shown in Fig. 1A, some foci persisted and we found that some of the cells had larger foci ($>1 \mu\text{m}$ in diameter) from 4 h after IR, compared to initial foci observed within 30 min ($\leq 0.5 \mu\text{m}$, Fig. 1B). Some of the persistent foci seemed to grow time-dependently up to 24 h after IR (Fig. 1B). Therefore, we measured diameter of each phosphorylated ATM focus at each time point (Fig. 1C). In unirradiated cells, 9.5 % of cells were foci-positive, however, large foci ($\geq 1.6 \mu\text{m}$) were frequently found

in the foci-positive cells, (Table 1 and Fig. 1C, control). At 1-2 h after IR, 100% of cells became foci positive. At these time points, many small foci, most of which diameter distributed between 0.4 to 1 μm , were observed in every interphase nucleus, and almost no large foci as was observed in the control cells were found (Table 1). Distribution of bars in histograms shift to right between 4 and 24 h after IR, indicating that diameter of the persistent foci increased time-dependently after IR, and thereafter, it does not change significantly (cf. Fig. 1C, 24 h and Fig. 1G, 1 Gy 48 h). We confirmed similar growth of the persistent phosphorylated ATM foci after IR in widely-used human primary fibroblasts, such as BJ, MRC-5, and WI38 (data not shown). The foci growth long after IR was also observed in persistent foci of Ser139-phosphorylated histone H2AX, MDC1, 53BP1, and NBS1 (Fig. 1D), and the grown foci of these proteins colocalized perfectly with the grown foci of phosphorylated ATM (Fig. 1D).

Next we examined dose-dependency of the growth of the persistent phosphorylated ATM foci in G0-irradiated normal human diploid cells. Percentage of cells with the large foci ($\geq 1.6 \mu\text{m}$) increased in a dose-dependent manner, and the average number of the large foci per cell also increased dose-dependently 48 h after IR

(Fig. 1E and 1F). However, we observed no significant difference in foci size distribution 48 h after 1-8 Gy (Fig. 1G).

3.2. Role of the growth of the persistent foci in IR-induced G1 arrest

To know whether the grown persistent foci inhibit G1/S progression, G0-synchronized normal human diploid cells were irradiated with 1 Gy of X-rays, then, cells were released from synchronization immediately after IR, by trypsinizing and replating cells at low density. Twenty-four hours after release, cells were fixed and subjected to immunofluorescence staining for phosphorylated ATM and replication protein A (RPA) (Fig. 2A). In this experimental setting, RPA-positive S-phase cells appeared from 24 h after release irrespective of irradiation. Twenty-four hours after release, av. 39% of unirradiated cells, and av. 25% of 1 Gy-irradiated cells became RPA-positive, respectively (Fig. 2A). In this analysis, we categorized phosphorylated ATM foci into two groups: small foci ($<1.6 \mu\text{m}$) and large foci ($\geq 1.6 \mu\text{m}$), because focus size has variety. In 1 Gy-irradiated RPA positive cells, the large foci of phosphorylated

ATM were rarely (0.9%) found, while the small foci were observed in 45.9% of the cells (Fig. 2A, right bar). Next, in Figure 2B, percentage of RPA positive cells with no foci was set for 100%, and relative percentage of RPA positive cells with the small foci or the large foci was shown, to make the effect of foci growth on S phase entry clearer. Compared to cells with no foci, much lower percentage (1.8%) of the large foci positive cells had RPA staining, while only slightly-decreased percentage (79%) of cells with the small foci were RPA positive (Fig. 2B). We performed the same assay by continuous BrdU-labeling, and confirmed that very few cells (0.9 %) with the large foci were labeled with BrdU (Fig. 2C). These results indicate that most of the cells with the large foci stayed in G1 phase, and did not progress into S, or G2/M phase because BrdU was continuously treated from immediately after synchronization release to the time of fixation. To further substantiate RPA/BrdU negative cells with the large foci stay in G1 phase, G2/M cells were identified by the signal of phosphorylated histone H3 at Ser10. Percentage of individual cell cycle phases were given in Table 2. Cells positive for RPA staining were judged as S phase cells. G2/M cells were positive for phosphorylated histone H3 at Ser10. And both RPA and phosphorylated histone H3 negative cells were

regarded as G1 phase cells. Percentages of S phase cells with the large foci were almost the same between control and 1 Gy-irradiated cells (0.1% and 0.2%, respectively), whereas the fraction of cells with the large foci was significantly increased in irradiated G1 cells, compared to that in control G1 cells. None of the large foci positive cells were observed in both control and irradiated G2/M cells. In contrast, S phase cells with the small foci increased by irradiation (6.9% to 10.6%), though total S phase cells decreased after irradiation (39.4% to 24.7%). G2/M cells with the small foci were rarely observed both in control and irradiated cells (1.6% and 1.3%, respectively).

3.3. Correlation between the growth of phosphorylated ATM foci and the level of p53 phosphorylation

To determine whether the growth of the persistent foci is involved in amplification of G1 checkpoint signals, we examined the relationship between phosphorylated ATM foci and Ser15-phosphorylation of p53 (Fig. 3). It is well documented that the level of p53 protein after IR shows oscillation caused by

MDM2-mediated autoregulatory feedback loop [27, 28]. Therefore, it is possible that we underestimate the effect of the foci growth on p53 phosphorylation due to low levels of p53 as a result of oscillation. To rule out the possibility, we used Nutlin-3, which stabilizes p53 through inhibition of p53-MDM2 binding, to make p53 levels constant in all cells (Fig. 3A) [29]. Furthermore, we used G0-synchronized cells to exclude the possibility of p53 phosphorylation by ATR in S phase. Intriguingly, we observed more p53 phosphorylation in cells with grown foci than in cells with small or no foci (Fig. 3B, HE49). We analyzed correlation between fluorescence intensity of nucleoplasmic phosphorylated p53 and fluorescence intensity of nucleoplasmic phosphorylated ATM, which represents the sum of each focus's fluorescence (Fig. 3C, HE49). On the whole, fluorescence intensity of phosphorylated ATM decreased time-dependently after IR, because the loss of fluorescence by foci disappearance surpassed the gain of fluorescence by growth of the persistent foci (Fig. 3C, HE49). Concomitantly, fluorescence intensity of phosphorylated p53 decreased time-dependently overall. However, in normal cells, some of the cells maintained strong fluorescence intensity of phosphorylated ATM and phosphorylated p53 until 24 h after 1 Gy, like cells at 2 h after

1 Gy, or 24 h after 6 Gy, though most of the initial phosphorylated ATM foci disappeared at this time. All of such cells had the large phosphorylated ATM foci ($\geq 1.6 \mu\text{m}$) (Fig. 3B, HE49, 24 h after IR). We also performed the same assay using primary fibroblasts derived from a Nijmegen breakage syndrome (NBS) patient, because it is previously reported that NBS cells have a partial defect in ATM autophosphorylation at Ser1981, p53 phosphorylation at Ser15, and G1 arrest (Fig. 3B and 3C, WG1799) [30-32]. In NBS cells, growth of the persistent phosphorylated ATM foci seemed to be impaired (Fig. 3B, WG1799). Concomitantly with the defective foci growth, intensity of both phosphorylated ATM and phosphorylated p53 in NBS cells was lower than that in normal cells throughout the time course, and almost no NBS cells maintained strong intensity of both proteins 24 h after 1 Gy (Fig. 3C, WG1799). Although we also observed lower induction of p53 phosphorylation in NBS cells by western blotting at 2, and 4 h after IR, the difference of p53 phosphorylation in normal and NBS cells at 8, and 24 h after IR could not be detected by this analysis, suggesting the importance of individual cell analysis in Fig. 3C (Fig. 3D and 3E). Next we investigated p53-phosphorylating ability of a single phosphorylated ATM focus at 24 h after 1 Gy of

X-rays in normal cells. We observed clear correlation between diameter of a single phosphorylated ATM focus and fluorescence intensity of nucleoplasmic phosphorylated p53 (Fig. 3F).

3.4. Defective growth of the persistent IR-induced foci in AT-, and NBS cells

Previous studies demonstrated that cells derived from AT-, or NBS patients show multiple cell cycle checkpoint defects, including G1 checkpoint [3, 4, 31-33]. And furthermore, ATM and NBS1, which are responsible gene products for the diseases, are the components of the persistent grown IR-induced foci as described above (Fig. 1D). Therefore, we next analyzed 53BP1 foci in AT (AT2KY and AT5BI) and NBS primary fibroblasts after 1 Gy of X-rays (Fig. 4). When unirradiated, larger percentage of these cells were positive for 53BP1 foci compared to normal human cells (AT2KY; 19%, AT5BI; 46%, WG1799; 33%, cf. HE49; 9.5%, data not shown), and average number of 53BP1 foci per nucleus in these unirradiated cells were more than that in normal cells (AT2KY; 0.22, AT5BI; 0.73, WG1799; 0.43, Fig. 4B. cf. HE49; 0.15). However, size of

53BP1 foci observed in unirradiated AT-, or NBS cells was smaller than those of normal cells (Fig. 4C, control). Furthermore, maximal number of 53BP1 foci per nucleus in 1 Gy-irradiated AT-, or NBS cells was less than that in normal cells (cf. 36.9 at 15 min after IR in HE49, 27.7 at 15 min after IR in AT2KY, 26.8 at 30 min after IR in AT5BI, and 19.7 at 1 h after IR in WG1799, Fig. 4A). Although foci size distribution was not significantly different between AT, NBS, and normal cells at 1-2 h after IR, growth of persistent foci from 4 h was less pronounced in AT and NBS cells. Defective growth of the persistent foci was most clearly observed 24 h after IR (Fig. 4C, 24 h and 4D). We next examined the relationship between focus size of phosphorylated ATM and S phase entry in NBS primary fibroblasts and normal human diploid cells (Table 3). G₀-synchronized WG1799 and HE49 cells were irradiated or unirradiated with 1 Gy of X-rays, and immediately released from synchronization. Twenty-four hours after release, cells were fixed and immunostained with phosphorylated ATM and RPA. In unirradiated RPA positive NBS cells, 37.1% of cells were foci positive, and all foci in these cells were the small foci. We did not observe a large focus in unirradiated RPA positive NBS cells. Although 1 Gy of X-rays increased the percentage of RPA positive cells with foci

(83.6%), all foci in the irradiated RPA positive NBS cells were the small foci, and no large foci were detected. In RPA negative NBS cells, only few large foci were observed in both control and 1 Gy-irradiated cells (1.4% and 1.3%, respectively), confirming that growth of the persistent phosphorylated ATM foci is impaired in NBS cells. This is in contrast to 21.6% of 1 Gy-irradiated RPA negative normal cells that had the large phosphorylated ATM foci.

3.5. Functional distinction between the large foci and the small foci

To determine functional distinction between the large foci and the small foci, we performed chemical intervention of the foci growth in the time interval after the appearance of the small foci but before the growth to the large foci (Fig. 5). To achieve this, we used KU55933 (KU), an established inhibitor of ATM kinase activity (Fig. 5A) [34]. KU was treated from 4 h after 1 Gy of X-rays, at which time, the growth of the persistent foci begins (Fig.1B and C). We analyzed foci of phosphorylated ATM 24 h after 1 Gy in normal human diploid cells, and found that the foci growth was

significantly inhibited by the KU treatment from 4 h to 24 h after IR (Fig. 5B and C). Importantly, the small phosphorylated ATM foci, whose diameter was $0.5 \pm 0.2 \mu\text{m}$, still remained (Fig. 5C). We also examined whether p53 was phosphorylated in cells with the persistent small phosphorylated ATM foci (Fig. 5D and E). Without KU treatment, significant nuclear fluorescence of Ser15-phosphorylated p53 was found specifically in cells with the large phosphorylated ATM (Fig. 5E, indicated by white arrows in left panel). In contrast, with the KU treatment, no apparent phosphorylation of p53 was detected, in spite of the presence of the small foci (Fig. 5E, cf. middle and right panels).

4. Discussion

Results in the present study strongly indicate that the persistent foci of checkpoint factors remaining long after IR should be distinguished from the initial foci formed immediately after IR, when considering G1 checkpoint activation. Previously, Pilch et al. described the growth of the initial foci of phosphorylated histone H2AX within 90 min after IR [35]. In our observation, not only the initial foci of phosphorylated H2AX, but also those of phosphorylated ATM and 53BP1 grew (data not shown). The foci growth we described in the present study follows the initial foci growth, however, importantly, the “later” growth occurs only in the persistent foci long time after IR. If the initial foci determined the cell fate, all cells would undergo G1 arrest even after very low doses of IR, because the initial foci appear and grow in all interphase cells irradiated (Table 1, and data not shown). However, G1 checkpoint is characterized by its slower activation and persistence, which are major differences from S, or G2/M checkpoint [36, 37]. Therefore, most of the initial foci disappear at the onset of G1 arrest (Fig. 1A). Inevitably, cells with a limited number of irreparable damage must possess a mechanism

to amplify G1 checkpoint signals. In fact, we found growth of the persistent IR-induced foci in normal human diploid cells. This observation led us to speculate that, even with a single persistent focus, DNA damage signal can be amplified sufficiently for G1 arrest by the growth of the persistent focus. As expected, G1 cells with grown phosphorylated ATM foci showed difficulty to progress into S phase (Fig. 2, Table 2 and 3). We confirmed significant correlation between diameter of a single persistent Ser1981-phosphorylated ATM focus and fluorescence intensity of Ser15-phosphorylated p53 in individual cells, indicating that the ability of a single phosphorylated ATM focus to phosphorylate p53 depends on focus growth (Fig. 3F). Furthermore, the treatment of an ATM specific inhibitor (KU55933) from 4 h after IR dramatically decreased p53 phosphorylation to control levels, though the small foci of phosphorylated ATM persisted for over 24 h (Fig. 5E). These results clearly indicate that the small phosphorylated ATM foci are insufficient for p53 phosphorylation, supporting our notion that the function of a phosphorylated ATM focus depends on its size. Interestingly, the growth of the persistent foci was severely compromised in AT-, and NBS cells, though the initial foci growth was apparently normal in both cells (Fig. 4C,

4D, and Table 3). Previous studies reported that IR-induced G1 arrest is abolished in AT cells, and partially compromised in NBS cells [3, 4, 31, 32]. Of note, $\geq 1.6 \mu\text{m}$ foci of phosphorylated ATM or 53BP1 were rarely observed in both cells. These results indicate that ATM and NBS1 are important for the growth of the persistent foci, and imply the biological significance of the $\geq 1.6 \mu\text{m}$ foci. Our results can be one of the explanations why G1 checkpoint is not fully activated in NBS cells. Namely, in NBS cells, potential of phosphorylated ATM foci to phosphorylate p53 is lowered because of the defective foci growth. However, greater number of the “smaller “ persistent foci, which is a result of inefficient DSB repair, may partially supplement impaired foci growth, that may result in partial defect of G1 arrest in NBS cells.

It is highly likely that other DNA damage checkpoint factors are involved, not only in the initial foci growth, but also the growth of the persistent foci presented here (Fig. 1D). In fact, as shown in Fig. 1D, all of the grown foci of phosphorylated H2AX, MDC1, 53BP1 were colocalized with the grown phosphorylated ATM foci. Recent studies demonstrated that MDC1 is important for maintenance of H2AX phosphorylation and phosphorylated H2AX foci, rather than initial phosphorylation and

foci formation [38]. Furthermore, although MDC1 does not affect autophosphorylation of ATM, foci formation of phosphorylated ATM is completely abrogated in MDC1 (-/-) MEFs and severely compromised in MDC1-shRNA-expressing cells [38, 39]. These results indicate the importance of multi-factorial complex in amplifying DNA damage checkpoint signals.

Recently, it is proposed that multiple DSBs are assembled at a single or a few site(s) to be repaired [40, 41]. It can be assumed that a grown persistent focus represents such a “repair center”. However, distribution of foci diameter 48 h after IR was similar between 1–8 Gy (Fig. 1G). If the grown persistent foci consisted of many DSBs, size of the foci would become larger dose-dependently. Furthermore, recent studies demonstrated that DSB ends or DSB-containing chromatin in mammalian cells exhibits limited mobility [42, 43]. Therefore, we concluded that the grown persistent focus does not represent a repair center.

We propose that the growth of the persistent focus of checkpoint factors is the mechanism that amplifies a signal from a single chromosome aberration to the sufficient levels for G1 arrest. The results in the present study suggest the extreme sensitivity of

G1 arrest, because a single grown persistent focus can execute G1 arrest. Considering the persistence of G1 arrest, we believe that the “growth of persistent foci” is a universal mechanism for tumor suppression, to permanently exclude cells with remaining DNA damage.

Acknowledgements

We appreciate Dr. Kenshi Komatsu (Kyoto University) for his kind gift, WG1799 cells. This work was supported by the 21st century Center Of Excellence (COE) program, Global COE program in Nagasaki University, and Grant-in-Aid for Scientific Research from Japan Society for the Promotion of Science.

References

- [1] K. Savitsky, A. Bar-Shira, S. Gilad, G. Rotman, Y. Ziv, L. Vanagaite, D.A. Tagle, S. Smith, T. Uziel, S. Sfez, M. Ashkenazi, I. Pecker, M. Frydman, R. Harnik, S.R. Patanjali, A. Simmons, G.A. Clines, A. Sartiel, R.A. Gatti, L. Chessa, O. Sanal, M.F. Lavin, N.G.J. Jaspers, A.M.R. Taylor, C.F. Arlett, T. Miki, S.M. Weissman, M. Lovett, F.S. Collins, Y. Shiloh, A single ataxia telangiectasia gene with a product similar to PI-3 kinase, *Science* 268 (1995) 1749-1753.
- [2] R.B. Setlow, Repair deficient human disorders and cancer, *Nature* 271 (1978) 713-717.
- [3] B.R. Young, R.B. Painter, Radioresistant DNA synthesis and human genetic diseases, *Hum. Genet.* 82 (1989) 113-117.
- [4] M.S. Meyn, Ataxia-telangiectasia and cellular response to DNA damage, *Cancer Res.* 55 (1995) 5991-6001.
- [5] M.B. Kastan, D.S. Lim, The many substrates and function of ATM, *Nat. Rev. Mol. Cell Biol.* 1 (2000) 179-186.
- [6] S. Banin, L. Moyal, S.Y. Shieh, Y. Taya, C.W. Anderson, L. Chessa, N.I.

- Smorodinsky, C. Prives, Y. Reiss, Y. Shiloh, Y. Ziv, Enhanced phosphorylation of p53 by ATM in response to DNA damage, *Science* 281 (1998) 1674-1677.
- [7] C.E. Canman, D.S. Lim, K.A. Cimprich, Y. Taya, K. Tamai, K. Sakaguchi, E. Appella, M.B. Kastan, J.D. Siliciano, Activation of the ATM kinase by ionizing radiation and phosphorylation of p53, *Science* 281 (1998) 1677-1679.
- [8] R. Melchionna, X.B. Chen, A. Blasina, C.H. McGowan, Threonine 68 is required for radiation-induced phosphorylation and activation of Cds1, *Nat. Cell Biol.* 2 (2000) 762-765.
- [9] D.S. Lim, S.T. Kim, B. Xu, R.S. Maser, J. Lin, J.H. Petrini, M.B. Kastan, ATM phosphorylates p95/nbs1 in an S-phase checkpoint pathway, *Nature* 404 (2000) 613-617.
- [10] M. Gatei, D. Young, K.M. Cerosaletti, A. Desai-Mehta, K. Spring, S. Kozlov, M.F. Lavin, R.A. Gatti, P. Concannon, K.K. Khanna, ATM-dependent phosphorylation of nibrin in response to radiation exposure, *Nat. Genet.* 25 (2000) 115-119.
- [11] S. Zhao, Y.C. Weng, S.S. Yuan, Y.T. Lin, H.C. Hsu, S.C. Lin, E. Gerbino, M.H. Song, M.Z. Zdzienicka, R.A. Gatti, J.W. Shay, Y. Ziv, Y. Shiloh, E.Y. Lee,

Functional link between ataxia-telangiectasia and Nijmegen breakage syndrome gene products, *Nature* 405 (2000) 473-477.

[12] X. Wu, V. Ranganathan, D.S. Weisman, W.F. Heine, D.N. Ciccone, T.B. O'Neill, K.E. Crick, K.A. Pierce, W.S. Lane, G. Rathbun, D.M. Livingston, D.T. Weaver, ATM phosphorylation of Nijmegen breakage syndrome protein is required in a DNA damage response, *Nature* 405 (2000) 477-482.

[13] C.J. Bakkenist, M.B. Kastan, DNA damage activates ATM through intermolecular autophosphorylation and dimer dissociation, *Nature* 421 (2003) 499-506.

[14] E.P. Rogakou, D.R. Pilch, A.H. Orr, V.S. Ivanova, W.M. Bonner, DNA double-stranded breaks induce histone H2AX phosphorylation on serine 139, *J. Biol. Chem.* 273 (1998) 5858-5868.

[15] S. Burma, B.P. Chen, M. Murphy, A. Kurimasa, D. Chen, ATM phosphorylates histone H2AX in response to DNA double-strand breaks, *J. Biol. Chem.* 276 (2001) 42462-42467.

[16] E.P. Rogakou, C. Boon, C. Redon, W.M. Bonner, Megabase chromatin domains involved in DNA double-strand breaks in vivo, *J. Cell Biol.* 146 (1999) 905-915.

- [17] O.A. Sedelnikova, E.P. Rogakou, I.G. Panyutin, W.M. Bonner, Quantitative detection of ¹²⁵IIdU-induced DNA double-strand breaks with γ -H2AX antibody, *Radiat. Res.* 158 (2002) 486-492.
- [18] K. Iwabuchi, P.L. Bartel, B. Li, R. Marraccino, S. Fields, Two cellular proteins that bind to wild-type but not mutant p53, *Proc. Natl. Acad. Sci. U.S.A.* 91 (1994) 6098-6102.
- [19] L.B. Schultz, N.H. Chehab, A. Malikzay, T.D. Halazonetis, p53-binding protein 1 (53BP1) is an early participant in the cellular response to DNA double-strand breaks, *J. Cell Biol.* 151 (2000) 1381-1390.
- [20] I. Rappold, K. Iwabuchi, T. Date, J. Chen, Tumor suppressor p53 binding protein 1 (53BP1) is involved in DNA damage-signaling pathways, *J. Cell Biol.* 153 (2001) 613-20.
- [21] M. Goldberg, M. Stucki, J. Falck, D. D'Amours, D. Rahman, D. Pappin, J. Bartek, S.P. Jackson, MDC1 is required for the intra-S-phase DNA damage checkpoint, *Nature* 421 (2003) 952-956.
- [22] O. Fernandez-Capetillo, H.T. Chen, A. Celeste, I. Ward, P.J. Romanienko, J.C.

- Morales, K. Naka, Z. Xia, R.D. Camerini-Otero, N. Motoyama, P.B. Carpenter, W.M. Bonner, J. Chen, A. Nussenzweig, DNA damage-induced G2/M checkpoint activation by histone H2AX and 53BP1, *Nat. Cell Biol.* 4 (2002) 993-997.
- [23] B. Wang, S. Matsuoka, P.B. Carpenter, S. Elledge, 53BP1, a mediator of the DNA damage checkpoint, *Science* 298 (2002) 1435-1438.
- [24] Z. Lou, K. Minter-Dykhouse, X. Wu, J. Chen, MDC1 is coupled to activated CHK2 in mammalian DNA damage response pathways, *Nature* 421 (2003) 957-961.
- [25] G.S. Stewart, B. Wang, C.R. Bignell, A.M.R. Taylor, S.J. Elledge, MDC1 is a mediator of the mammalian DNA damage checkpoint, *Nature* 421 (2003) 961-966.
- [26] C. Lukas, J. Falck, J. Bartkova, J. Bartek, J. Lukas, Distinct spatiotemporal dynamics of mammalian checkpoint regulators induced by DNA damage, *Nat. Cell Biol.* 5 (2003) 255-260.
- [27] R.L. Bar-Or, R. Maya, L.A. Segel, U. Alon, A.J. Levine, M. Oren, Generation of oscillations by the p53-Mdm2 feedback loop: A theoretical and experimental study, *Proc. Natl. Acad. Sci. U.S.A.* 97 (2000) 11250-11255.

- [28] J.C. Ghosh, Y. Izumida, K. Suzuki, S. Kodama, M. Watanabe, Dose-dependent biphasic accumulation of TP53 protein in normal human embryo cells after X irradiation, *Radiat. Res.* 153 (2000) 305-311.
- [29] L.T. Vassilev, B.T. Vu, B. Graves, D. Carvajal, F. Podlaski, Z. Filipovic, N. Kong, U. Kammlott, C. Lukacs, C. Klein, N. Fotouhi, E.A. Liu, In vivo activation of the p53 pathway by small-molecule antagonists of MDM2, *Science* 303 (2004) 844-848.
- [30] T. Uziel, Y. Lerenthal, L. Moyal, Y. Andegeko, L. Mittelman, Y. Shiloh, Requirement of the MRN complex for ATM activation by DNA damage, *EMBO J.* 22 (2003) 5612-5621.
- [31] P.M. Girard, E. Riballo, A.C. Begg, A. Waugh, P.A. Jeggo, Nbs1 promotes ATM dependent phosphorylation events including those required for G1/S arrest, *Oncogene* 21 (2002) 4191-4199.
- [32] W. Jongmans, M. Vuillaume, K. Chrzanowska, D. Smeets, K. Sperling, J. Hall, Nijmegen breakage syndrome cells fail to induce the p53-mediated DNA damage response following exposure to ionizing radiation, *Mol. Cell Biol.* 17 (1997)

5016-5022.

[33] G. Buscemi, C. Savio, L. Zannini, F. Micciche, D. Masnada, M. Nakanishi, H.

Tauchi, K. Komatsu, S. Mizutani, K.K. Khanna, P. Chen, P. Concannon, L.

Chessa, D. Delia, Chk2 activation dependence on Nbs1 after DNA damage, *Mol.*

Cell Biol. 21 (2001) 5214-5222.

[34] I. Hickson, Y. Zhao, C.J. Richardson, S.J. Green, N.M.B. Martin, A.I. Orr,

P.M.Reaper, S.P. Jackson, N.J. Curtin, G.C.M. Smith, Identification and

characterization of a novel and specific inhibitor of the ataxia-telangiectasia

mutated kinase ATM, *Cancer Res.* 64 (2004) 9152-9159.

[35] D.R. Pilch, O.A. Sedelnikova, C. Redon, A. Celeste, A. Nussenzweig, W.M.

Bonner, Characteristics of γ -H2AX foci at DNA double-strand break sites,

Biochem. Cell Biol. 81 (2003) 123-129.

[36] A. Di Leonardo, S.P. Linke, K. Clarkin, G.M. Wahl, DNA damage triggers a

prolonged p53-dependent G₁ arrest and long-term induction of Cip1 in normal

human fibroblasts, *Genes Dev.* 8 (1994) 2540-2551.

[37] K. Suzuki, I. Mori, Y. Nakayama, M. Miyakoda, S. Kodama, M. Watanabe,

Radiation-induced senescence-like growth arrest requires TP53 function but not telomere shortening, *Radiat. Res.* 155 (2001) 248-253.

- [38] M. Stucki, J.A. Clapperton, D. Mohammad, M.B. Yaffe, S.J. Smerdon, S.P. Jackson, MDC1 directly binds phosphorylated histone H2AX to regulate cellular responses to DNA double-strand breaks, *Cell* 123 (2005) 1213-1226.
- [39] Z. Lou, K. Minter-Dykhouse, S. Franco, M. Gostissa, M.A. Rivera, A. Celeste, J.P. Manis, J. van Deursen, A. Nussenzweig, T.T. Paull, F.W. Alt, J. Chen, MDC1 maintains genomic stability by participating in the amplification of ATM-dependent DNA damage signals, *Mol. Cell* 21 (2006) 187-200.
- [40] J.A. Aten, J. Stap, P.M. Krawczyk, C.H. van Oven, R.A. Hoebe, J. Essers, R. Kanaar, Dynamics of DNA double-strand breaks revealed by clustering of damaged chromosome domains, *Science* 303 (2004) 92-95.
- [41] M. Lisby, U.H. Mortensen, R. Rothstein, Colocalization of multiple DNA double-strand breaks at a single Rad52 repair centre, *Nat. Cell Biol.* 5 (2003) 572-577.
- [42] E. Soutoglou, J.F. Dorn, K. Sengupta, M. Jasin, A. Nussenzweig, T. Ried, G.

Danuser, and T. Misteli, Positional stability of single double-strand breaks in mammalian cells, *Nat. Cell Biol.* 9 (2007) 675-682.

[43] M.J. Kruhlak, A. Celeste, G. Dellaire, O. Fernandez-Capetillo, W.G. Muller, J.G.

McNally, D.P. Bazett-Jones, A. Nussenzweig, Changes in chromatin structure and mobility in living cells at sites of DNA double-strand breaks, *J. Cell Biol.* 172 (2006) 823-834.

Figure legends

Figure 1. Growth of persistent IR-induced foci in normal human diploid cells.

(A) Kinetics of phosphorylated ATM foci number after IR. HE49 cells were unirradiated (C) or irradiated with 1 Gy of X-rays, and then, fixed at indicated time points, followed by immunofluorescence staining for phosphorylated ATM (Ser1981). More than 100 cells were analyzed at each time point. The average number of foci per nucleus was calculated, and indicated above the bars in the graph.

(B) Growth of the persistent phosphorylated ATM foci. HE49 cells were unirradiated (C) or irradiated with 1 Gy of X-rays and fixed at indicated time points, followed by immunofluorescence staining for phosphorylated ATM (Ser1981, red). Nucleus was counterstained with DAPI (blue).

(C) Kinetics of foci size distribution of phosphorylated ATM after IR. HE49 cells were unirradiated (C) or irradiated with 1 Gy of X-rays and fixed at indicated time points, followed by immunofluorescence staining for phosphorylated ATM (Ser1981). Diameter of phosphorylated ATM foci was measured as described in *Materials and Methods*. Data were obtained from more than 100 foci positive cells at each time point.

(D) Growth of the persistent foci of other checkpoint factors. HE49 cells were irradiated with 1 Gy of X-rays and fixed 24 h later, followed by immunofluorescence staining for phosphorylated ATM (Ser1981, green) and phosphorylated histone H2AX (Ser139), MDC1, 53BP1, or NBS1 (red). Nucleus was counterstained with DAPI (blue).

(E) Dose-dependency of the percentage of the large phosphorylated ATM foci positive cells. G0-synchronized HE49 cells were unirradiated or irradiated with 1, 2, 4, 6, or 8 Gy of X-rays, then, replated onto coverslips and fixed 48 h later, followed by immunofluorescence staining for phosphorylated ATM (Ser1981). Foci of 1.6 μm or more in diameter were counted as the large foci. Focus diameter measurement was performed as described in *Materials and Methods*. Data were obtained from more than 100 cells at each dose.

(F) Dose-dependency of the average number of the large phosphorylated ATM foci per cell. Sample preparation and analysis were performed as described in (E). Data were obtained from more than 100 cells at each dose.

(G) Distribution of foci size after different doses of X-rays. Sample preparation and analysis were performed as described in (E). Data were obtained from more than 100

foci positive cells at each dose.

Figure. 2. Correlation between the growth of the persistent phosphorylated ATM foci and G1 arrest.

(A) Percentage of cells with no focus, small focus ($<1.6 \mu\text{m}$), or large focus ($\geq 1.6 \mu\text{m}$) in RPA positive cells. G0-synchronized HE49 cells were unirradiated (control), or irradiated with 1 Gy of X-rays and then, immediately released from synchronization. Twenty-four hours after release, cells were fixed, followed by immunofluorescence staining for phosphorylated ATM (Ser1981) and RPA. RPA was stained to detect S phase cells. Most grown focus in each cell was analyzed, and focus diameter was measured as described in *Materials and Methods*. Average percentage from three independent experiments is shown. Data were obtained from more than 200 cells in each experiment.

(B) Relative efficiency of S phase entry in cells with the small, or the large phosphorylated ATM foci. The same data as in (A) were used in this analysis. The percentage of RPA positive cells without a focus was set for 100%, and the relative

average percentage of RPA positive cells with the small ($<1.6 \mu\text{m}$) or the large ($\geq 1.6 \mu\text{m}$) focus was indicated.

(C) Percentage of cells with no focus, small focus ($<1.6 \mu\text{m}$), or large focus ($\geq 1.6 \mu\text{m}$) in BrdU positive cells. G₀-synchronized HE49 cells were unirradiated (control), or irradiated with 1 Gy of X-rays and then, immediately released from synchronization. At the time of release, cells were replated into media containing 0.5 mM BrdU, and then, cells were incubated with the media until fixation. Twenty-four hours after release, cells were fixed, followed by immunofluorescence staining for phosphorylated ATM (Ser1981) and BrdU. Most grown focus in each cell was analyzed, and focus diameter was measured as described in *Materials and Methods*. Data were obtained from more than 200 cells.

(D) Relative efficiency of S phase entry in cells with the small, or the large phosphorylated ATM foci. The same data as in (C) were used in this analysis. The percentage of BrdU positive cells without a focus was set for 100%, and the relative percentage of BrdU positive cells with the small ($<1.6 \mu\text{m}$) or the large ($\geq 1.6 \mu\text{m}$) focus was indicated.

Figure 3. Correlation between the growth of the persistent phosphorylated ATM foci and the level of p53 phosphorylation at Ser15.

(A) Schematic representation of experimental procedures in Figure 3.

(B) Immunofluorescence images of phosphorylated ATM foci and Ser15-phosphorylated p53 after IR. G0-synchronized HE49 cells or WG1799 cells pretreated with 8 μ M Nutlin-3 were irradiated with 1 Gy of X-rays, then replated, and fixed at indicated time points, followed by immunofluorescence staining for phosphorylated ATM (Ser1981, green) and phosphorylated p53 (Ser15, red). Nucleus was counterstained with DAPI (blue). Note that the strong fluorescence intensity of Ser15-phosphorylated p53 is specifically observed in normal cells with grown phosphorylated ATM foci at 8, or 24 h after IR.

(C) Correlation between nucleoplasmic fluorescence intensity of phosphorylated ATM and that of phosphorylated p53. Fluorescence intensity of both proteins was measured as described in *Materials and Methods*. Data were obtained from more than 100 cells at each time point.

(D) p53 phosphorylation at Ser15 after 1 Gy of X-rays in normal and NBS cells.

G0-synchronized HE49 or WG1799 cells were pretreated with 32 μ M Nutlin-3 for 24 h, followed by 1 Gy irradiation. Cells were harvested at indicated time points, and were subjected to western blotting for Ser15-phosphorylated p53, p53, and α -tubulin (loading control).

(E) Induced level of p53 phosphorylation. Band intensity of Ser15-phosphorylated p53 in (D) was measured using NIH image.

(F) Correlation between diameter of a single phosphorylated ATM focus and fluorescence intensity of phosphorylated p53. G0-synchronized HE49 cells pretreated with 8 μ M Nutlin-3 were irradiated with 1 Gy of X-rays, then replated, and fixed at 24 h after IR, followed by immunofluorescence staining for phosphorylated ATM (Ser1981) and phosphorylated p53 (Ser15). Focus diameter and fluorescence intensity were measured as described in *Materials and Methods*. Data were obtained from more than 100 cells with a single phosphorylated ATM focus.

Figure 4. Defective growth of the persistent 53BP1 foci in AT-, and NBS cells after IR.

(A) Kinetics of 53BP1 foci number in AT, NBS, and normal cells after IR. AT2KY,

AT5BI, WG1799, and HE49 cells were unirradiated (0), or irradiated with 1 Gy of X-rays and fixed at indicated time points. After fixation, cells were stained for 53BP1. In the graph, average foci number calculated from more than 100 cells was plotted at each time point.

(B) Number of 53BP1 foci in unirradiated AT, NBS, and normal cells. Each bar graph shows average foci number calculated from more than 100 cells.

(C) Kinetics of foci size distribution of 53BP1 in AT, NBS, and normal cells after IR.

AT2KY, AT5BI, WG1799, and HE49 cells were unirradiated (C) or irradiated with 1 Gy of X-rays, and fixed at indicated time points. After fixation, cells were stained for 53BP1. Focus diameter measurement was performed as described in *Materials and Methods*. Data were obtained from more than 100 foci positive cells at each time point.

(D) Immunofluorescence images of the persistent 53BP1 foci in AT, NBS, and normal cells after IR. AT2KY, AT5BI, WG1799, and HE49 cells were irradiated with 1 Gy of X-rays, and fixed 24 h later. After fixation, cells were stained for 53BP1 (green). Nucleus was counterstained with DAPI (blue). Cells with typical number and size of 53BP1 foci are shown.

Figure 5. ATM-kinase-dependent foci growth and foci-size-dependent p53 phosphorylation.

(A) Schematic representation of experimental procedures. G0-synchronized HE49 cells were irradiated with 1 Gy of X-rays. From 4 h after IR to the time of fixation, 10 μ M KU55933 was either treated or mock-treated. Twenty-four hours after IR, cells were fixed, followed by immunofluorescence staining for phosphorylated ATM (Ser1981).

(B) Images of typical foci of phosphorylated ATM with or without KU treatment.

(C) Mean foci diameter of phosphorylated ATM with or without KU treatment. Mean foci diameter was measured as described in *Materials and Methods*. The data were obtained from more than 50 foci in more than 50 nuclei.

(D) Schematic representation of experimental procedures. G0-synchronized HE49 cells were pretreated with 8 μ M Nutlin-3 for 24 h, then irradiated with 1 Gy of X-rays. From 4 h after IR to the time of fixation, 10 μ M KU55933 was either treated or mock-treated. Twenty-four hours after IR, cells were fixed, followed by immunofluorescence staining for phosphorylated ATM (Ser1981) and phosphorylated p53 (Ser15).

(E) Images of typical phosphorylated ATM foci and phosphorylated p53. Control cells

(right panel) were treated only with 8 μ M nutlin-3, and were not exposed to KU55933 and X-rays. White arrows in left panel indicate cells positive for phosphorylation of p53 at Ser15 with the large phosphorylated ATM foci in non-KU-treated irradiated cells, which were not found in KU-treated irradiated cells (middle) and control cells (right).

Table 1. Kinetics of the percentage of cells with phosphorylated ATM foci or large phosphorylated ATM foci after IR. HE49 cells were unirradiated (C) or irradiated with 1 Gy of X-rays and fixed at indicated time points. After fixation, immunofluorescence staining was performed for phosphorylated ATM (Ser1981). Foci of 1.6 μ m or more in diameter were counted as the large foci.

Table 2. Inhibition of cell cycle progression at G1/S by the large foci. G0-synchronized HE49 cells were unirradiated (control) or irradiated with 1 Gy of X-rays. Immediately after irradiation, cells were released from synchronization, and fixed 24 h after release, followed by immunofluorescence staining for phosphorylated ATM (Ser1981) and RPA or phosphorylated histone H3 (Ser10). In this table, total number of analyzed cells was

set for 100%. Percentage of S phase cells or G2/M cells was calculated by counting RPA positive cells or phosphorylated histone H3 positive cells, respectively. Percentage of G1 cells was calculated by subtracting the percentage of RPA, and phosphorylated H3 positive cells from the percentage of cells with each foci status. Data were obtained from more than 500 cells.

Table 3. Relationship between focus size of phosphorylated ATM and G1/S progression in NBS and normal cells. G0-synchronized WG1799 or HE49 cells were unirradiated (control), or irradiated with 1 Gy of X-rays and then, immediately released from synchronization. Twenty-four hours after release, cells were fixed, followed by immunofluorescence staining for phosphorylated ATM (Ser1981) and RPA. Most grown focus in the nucleus was analyzed, and focus diameter was measured as described in *Materials and Methods*. Average percentage from three independent experiments is shown. Data were obtained from more than 200 cells in each experiment.

Figure 1

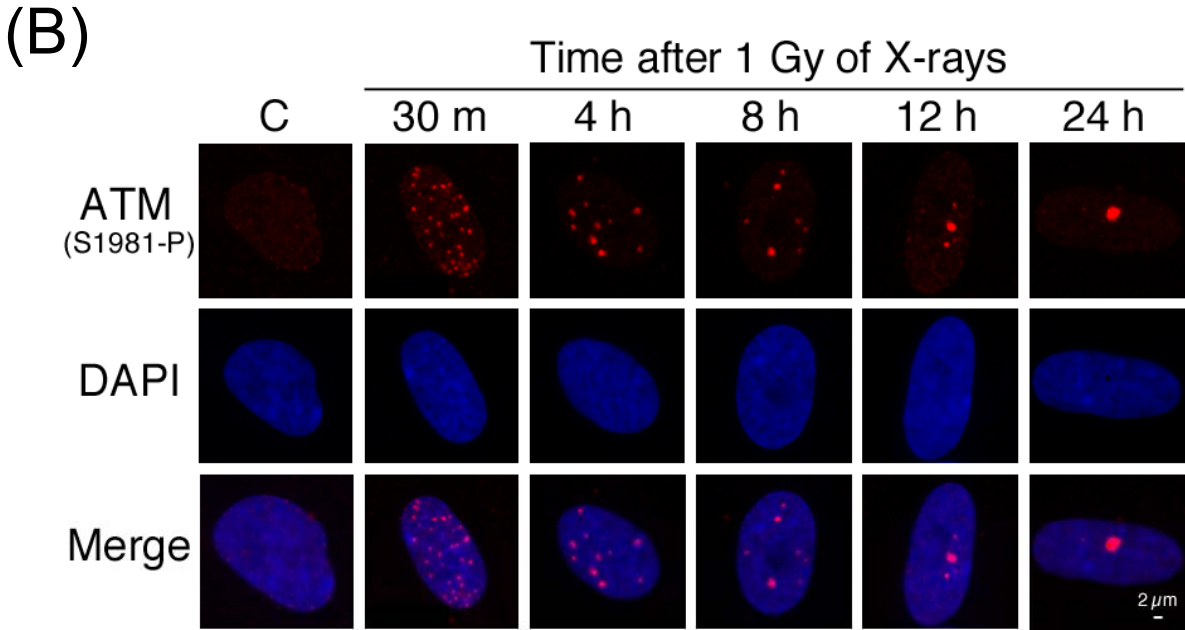
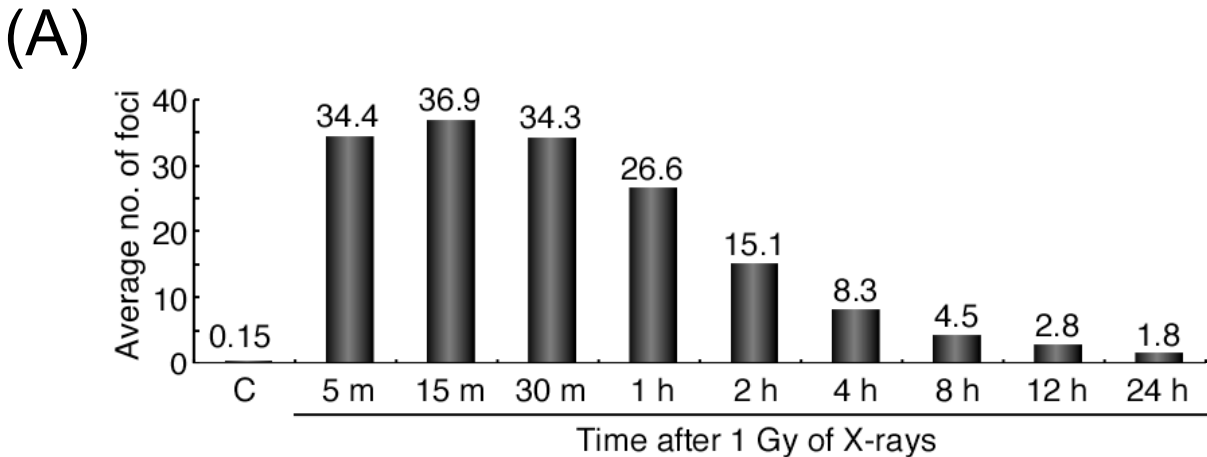


Figure 1

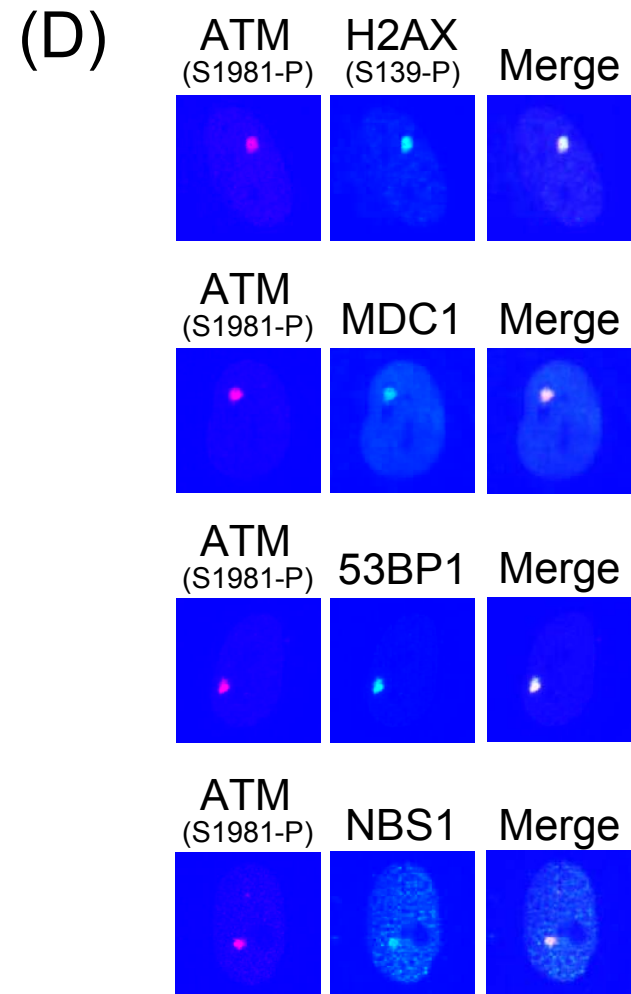
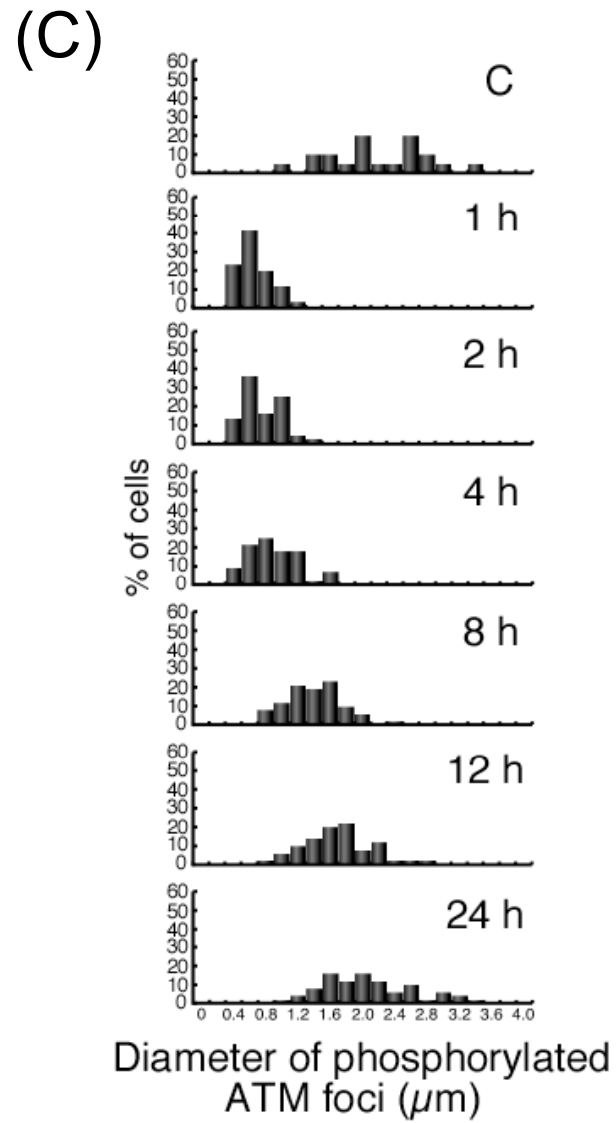


Figure 1

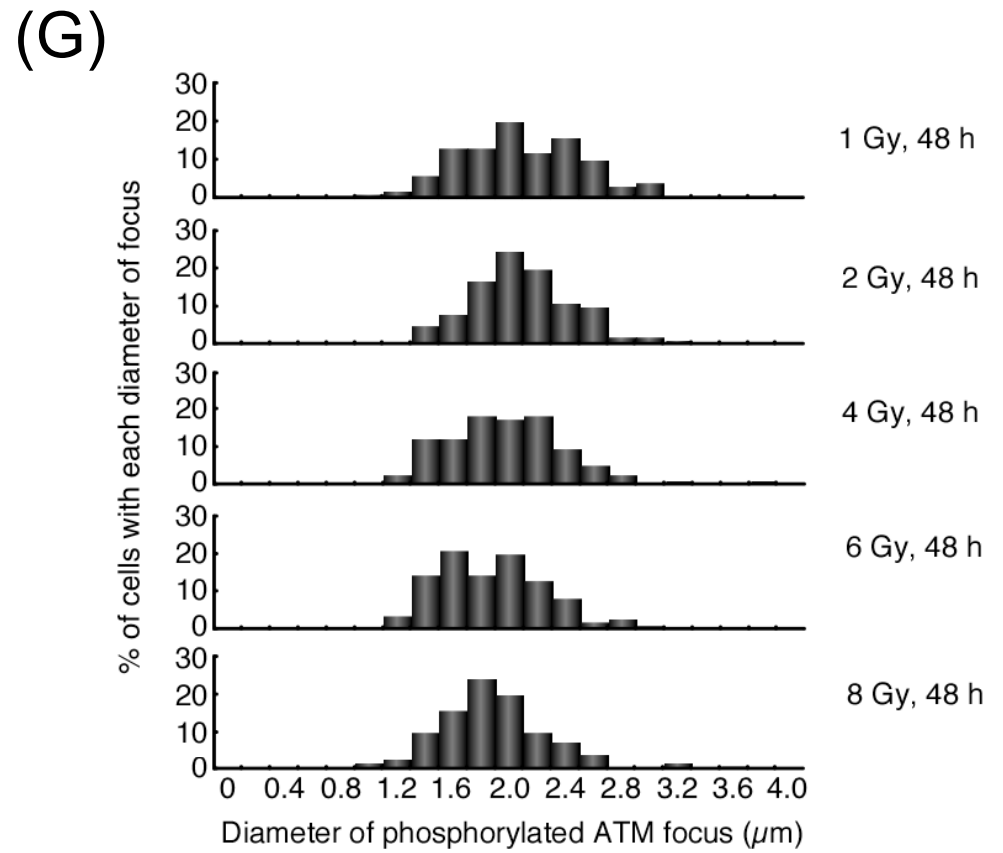
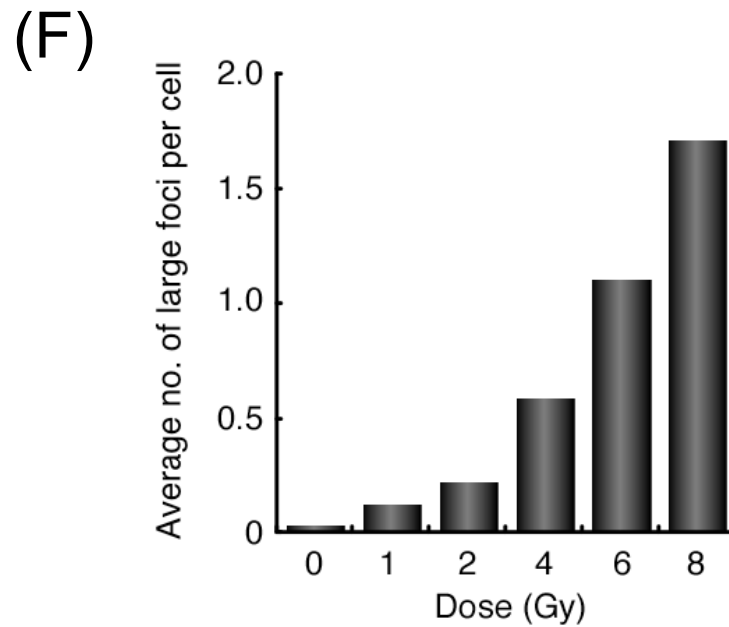
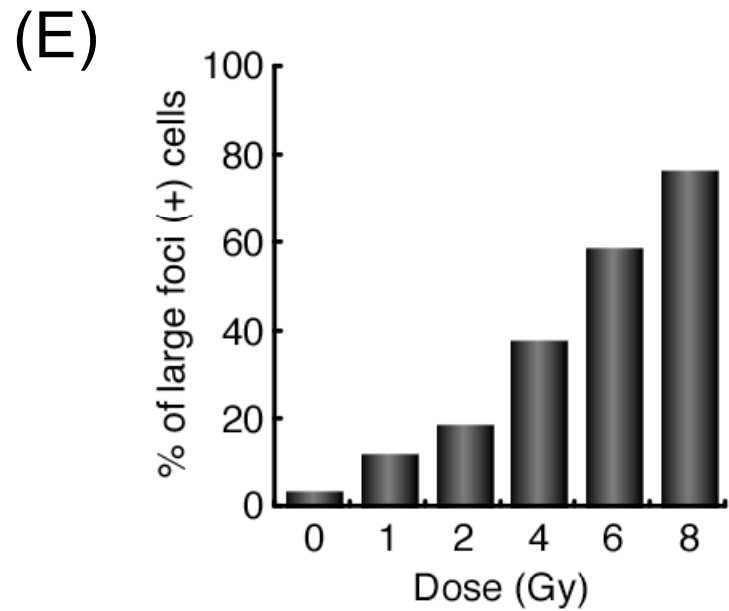
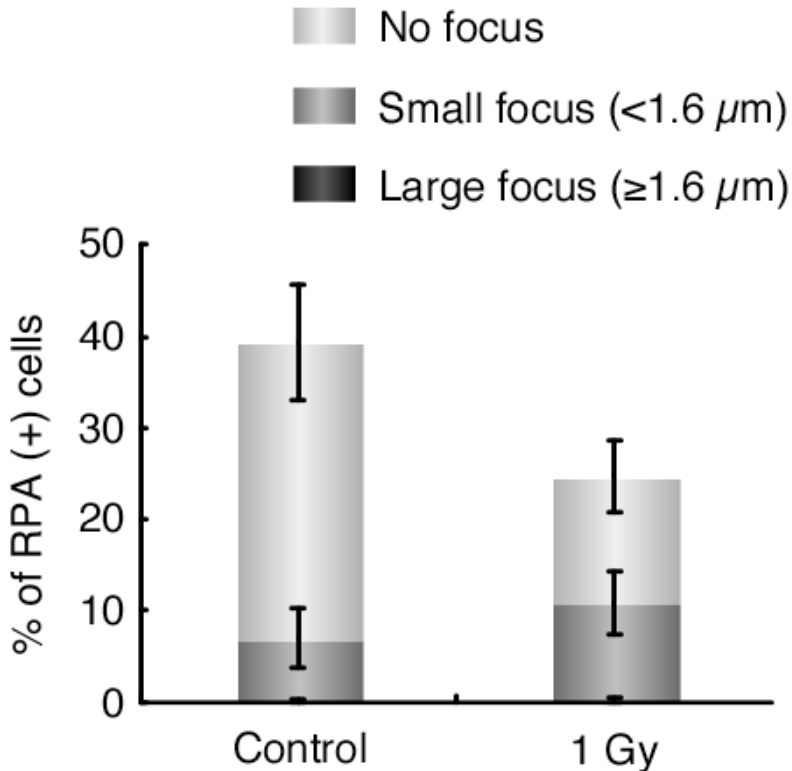


Figure 2

(A)



(B)

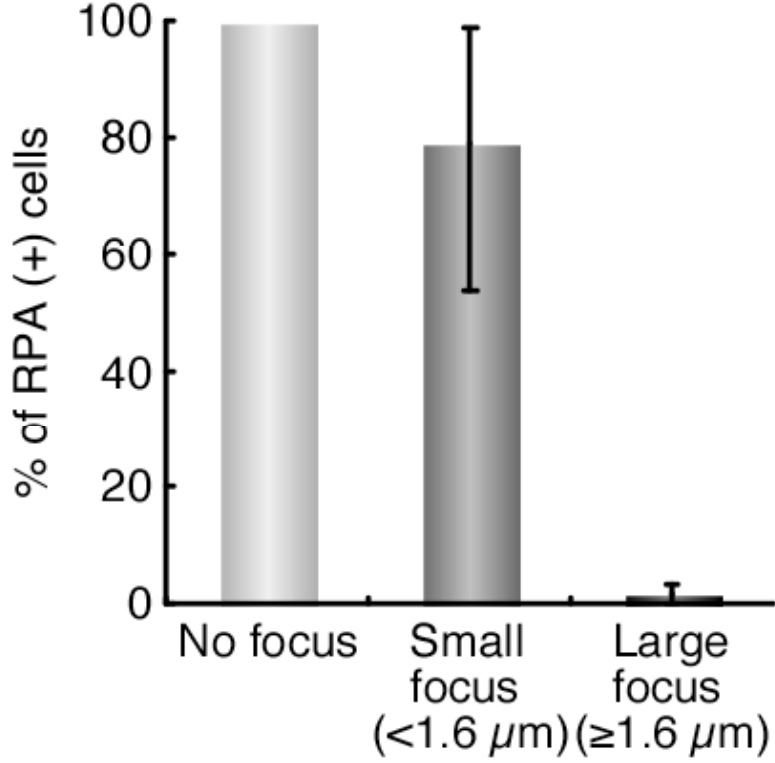
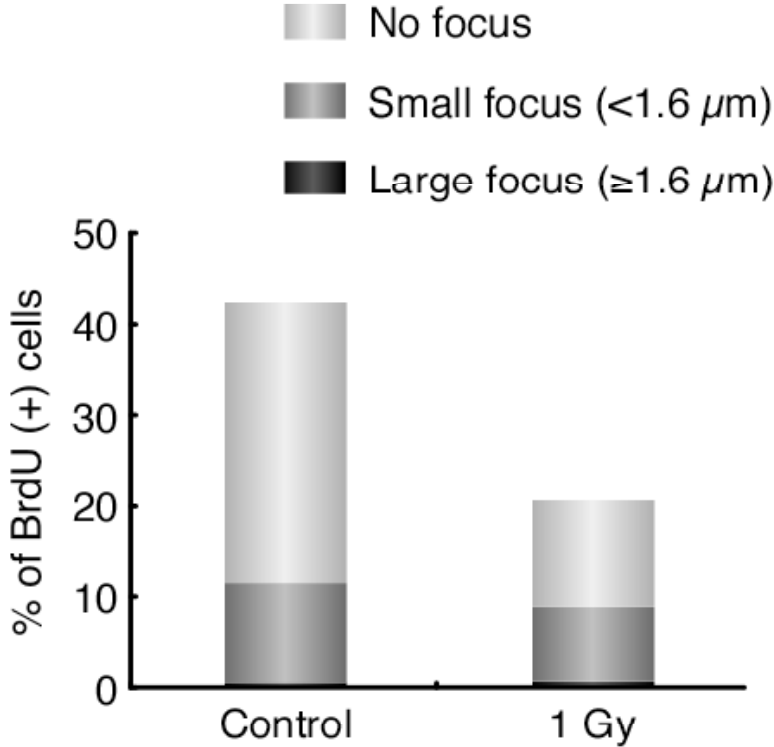


Figure 2

(C)



(D)

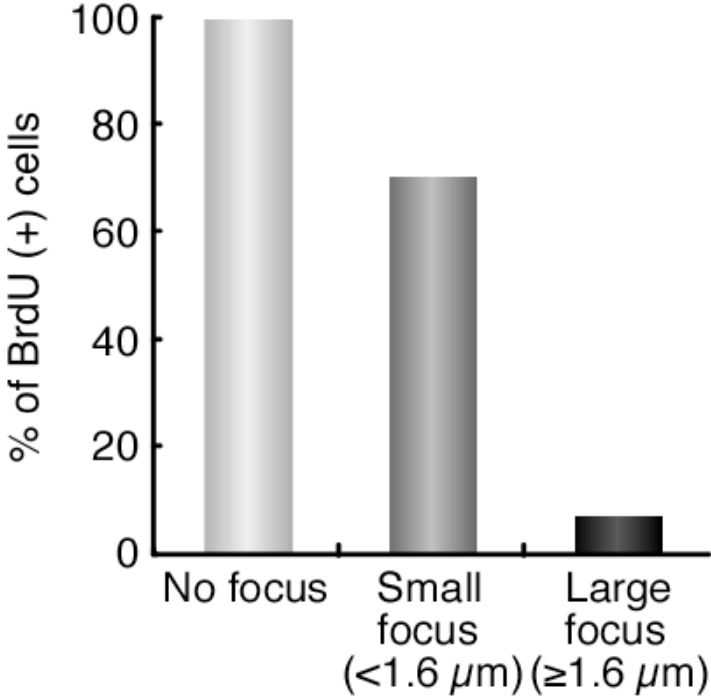
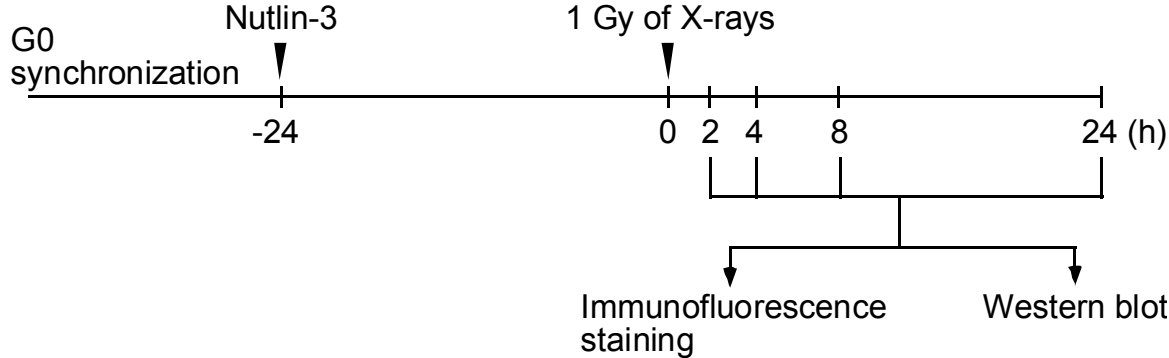
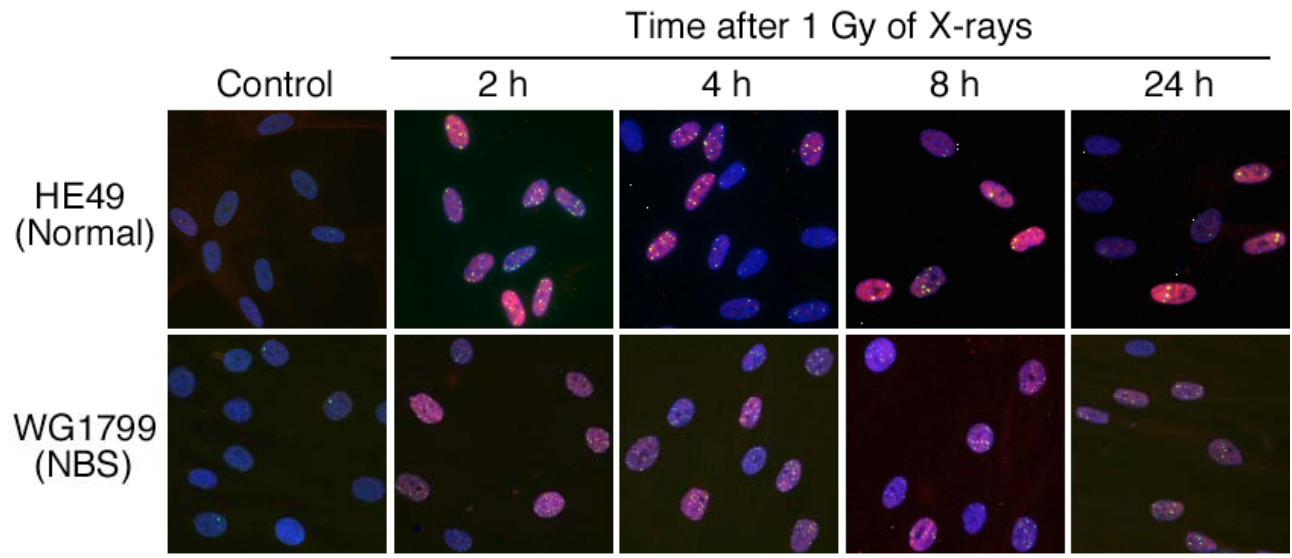


Figure 3

(A)



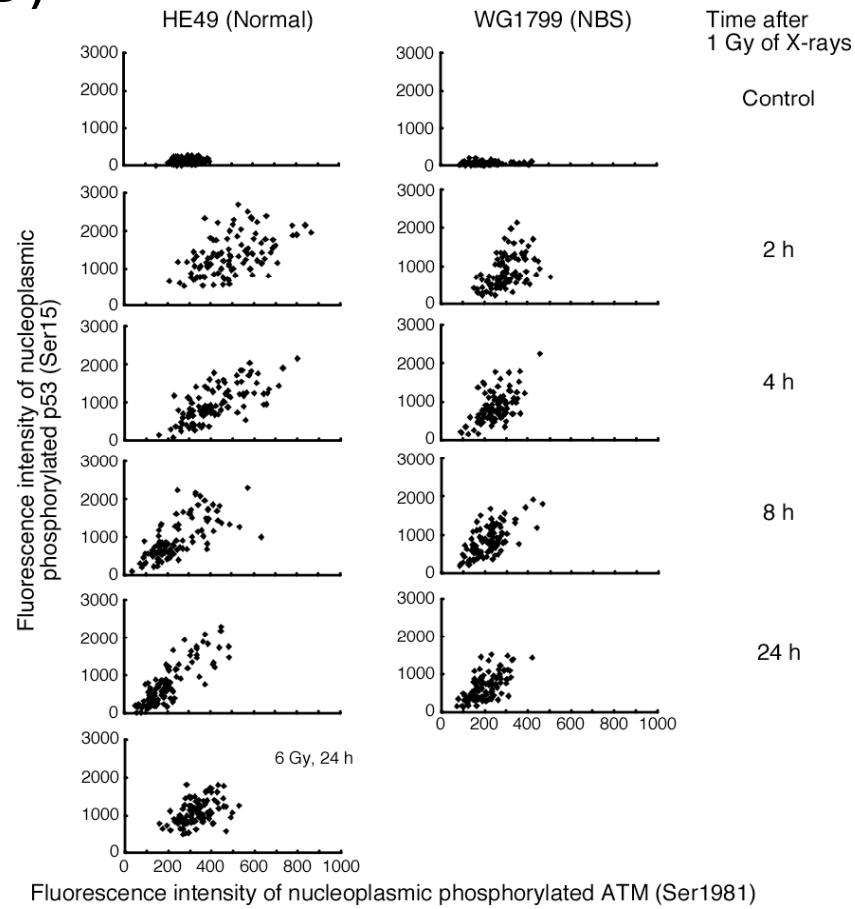
(B)



Green : Phosphorylated ATM (Ser1981)
Red : Phosphorylated p53 (Ser15)
Blue : DAPI

Figure 3

(C)



(D)

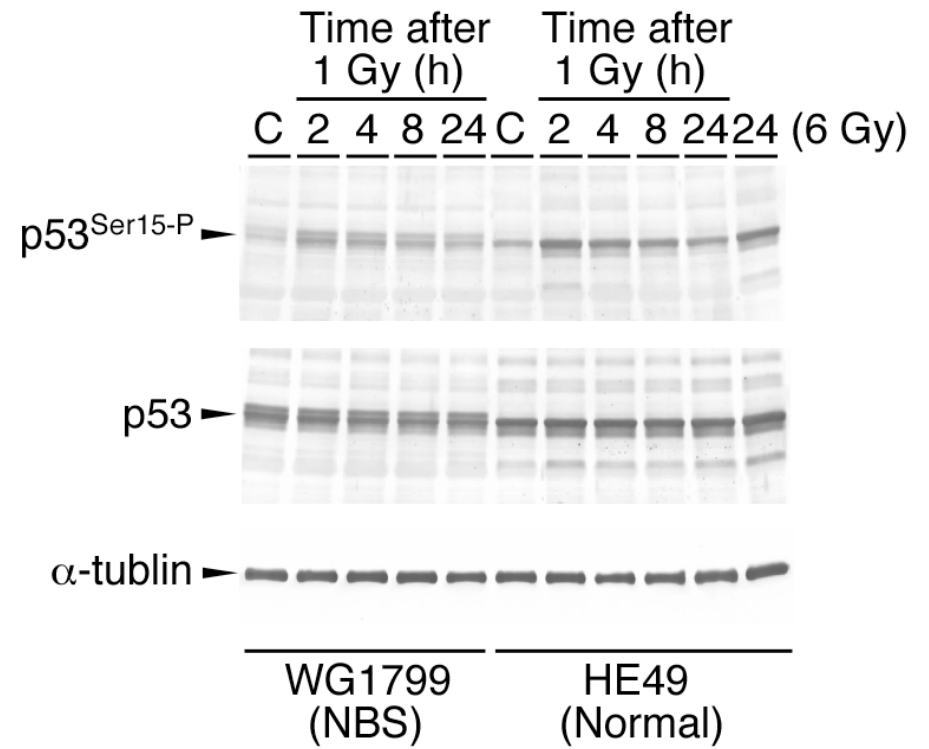
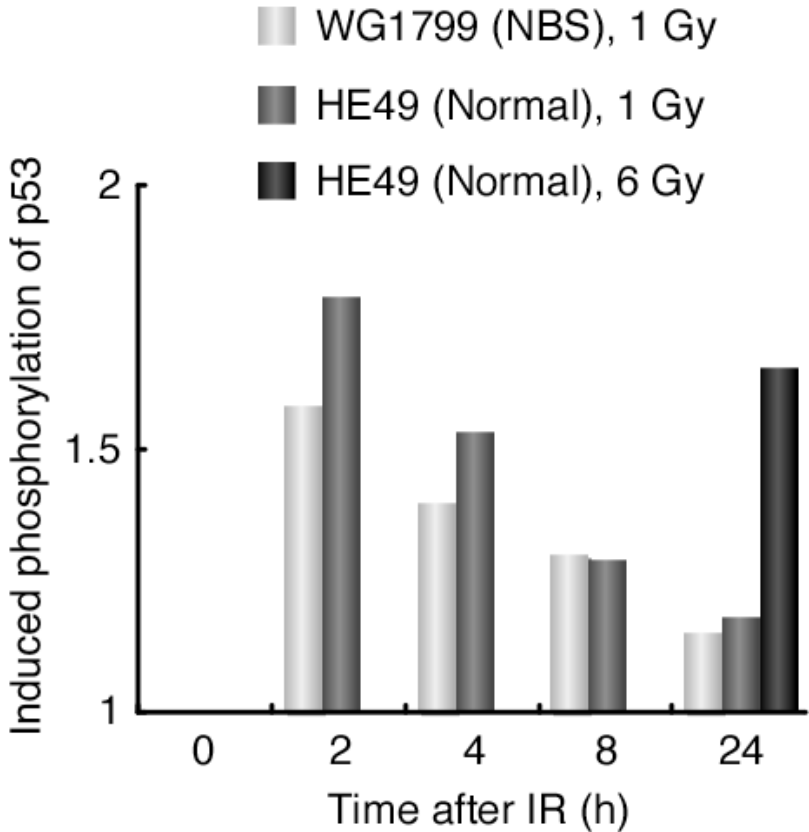


Figure 3

(E)



(F)

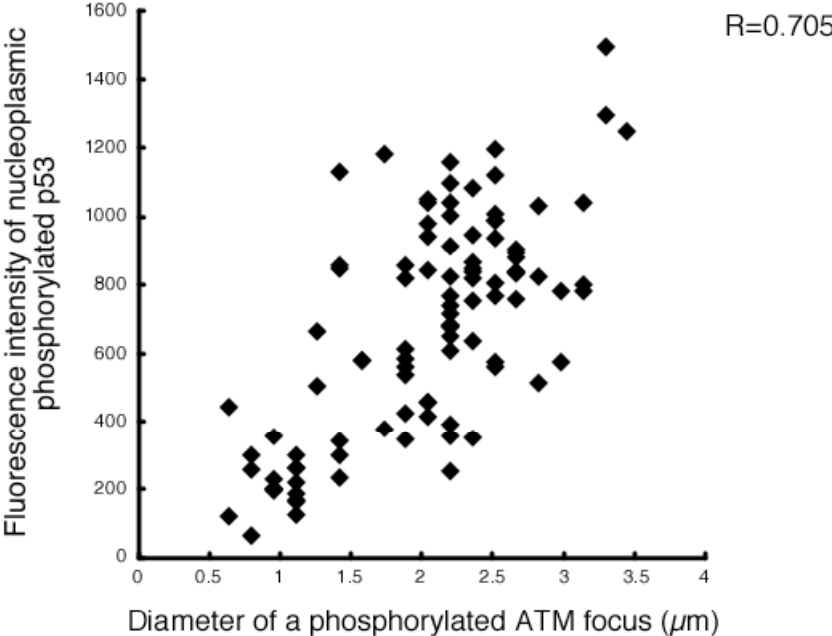
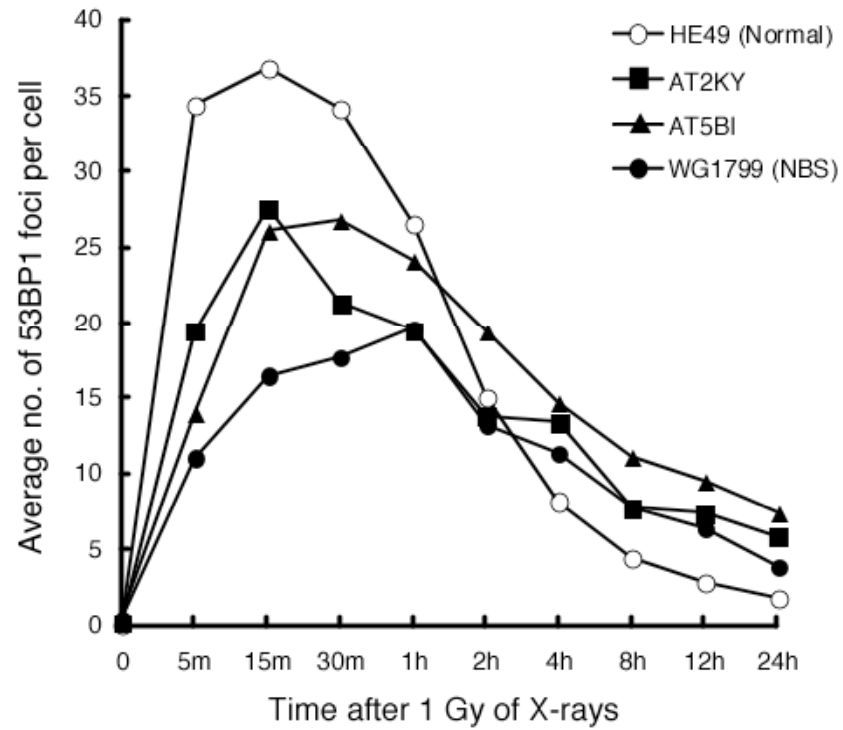


Figure 4

(A)



(B)

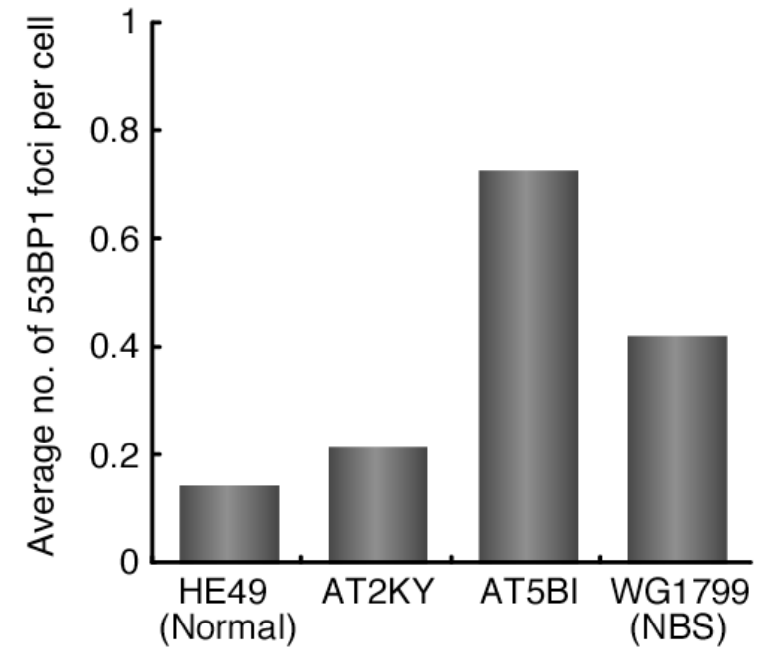


Figure 4

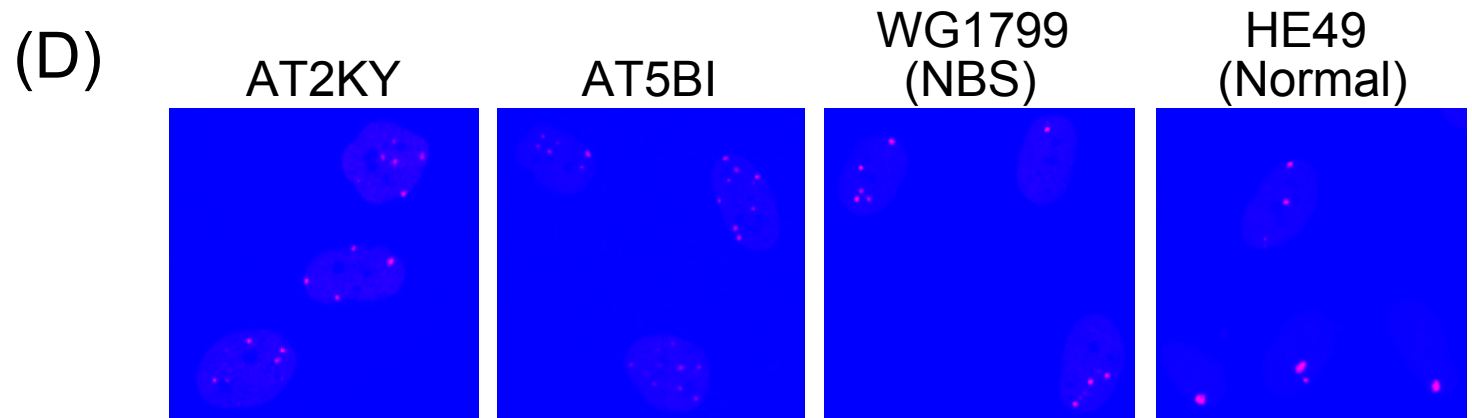
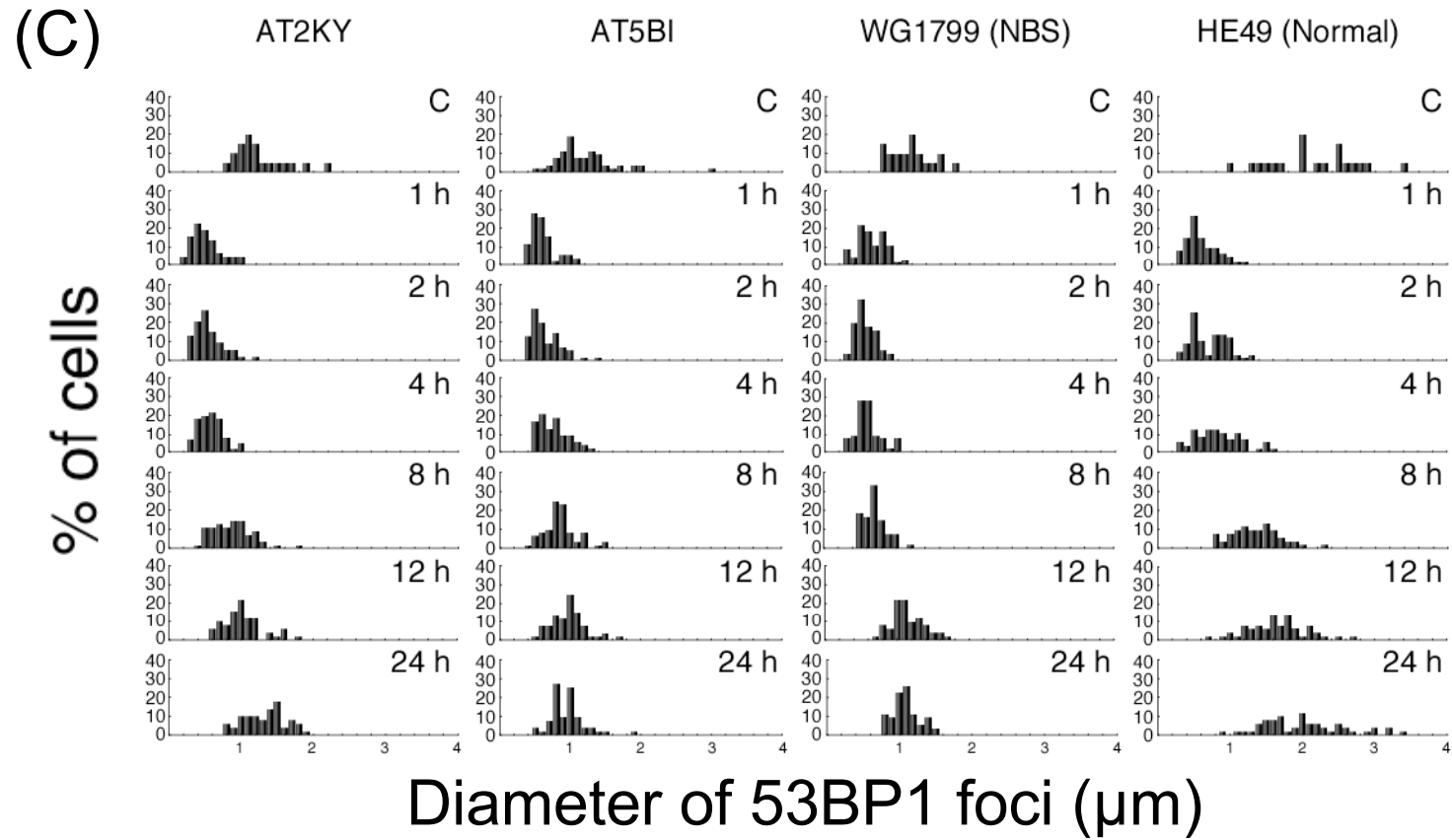
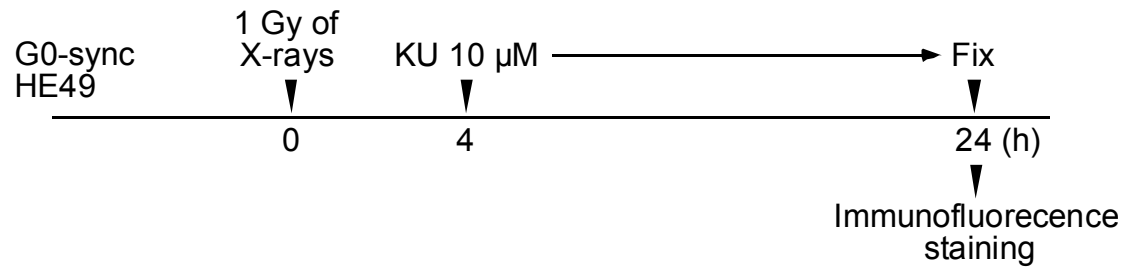
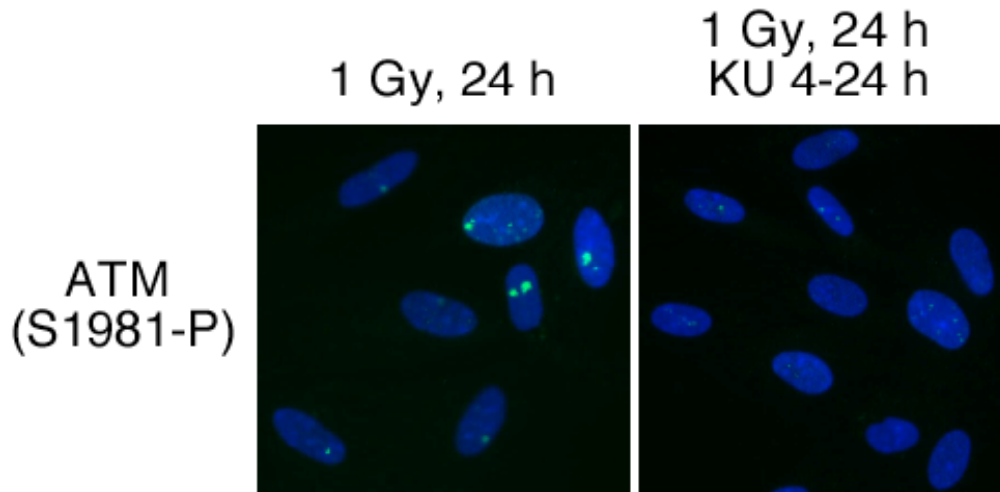


Figure 5

(A)



(B)

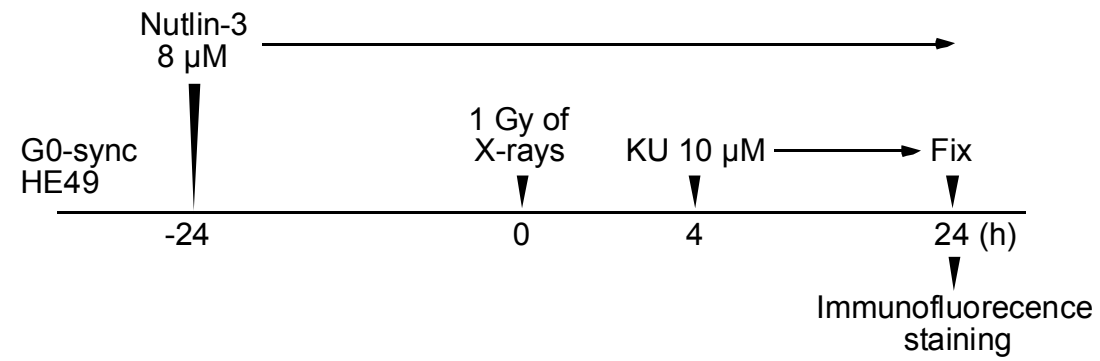


(C)

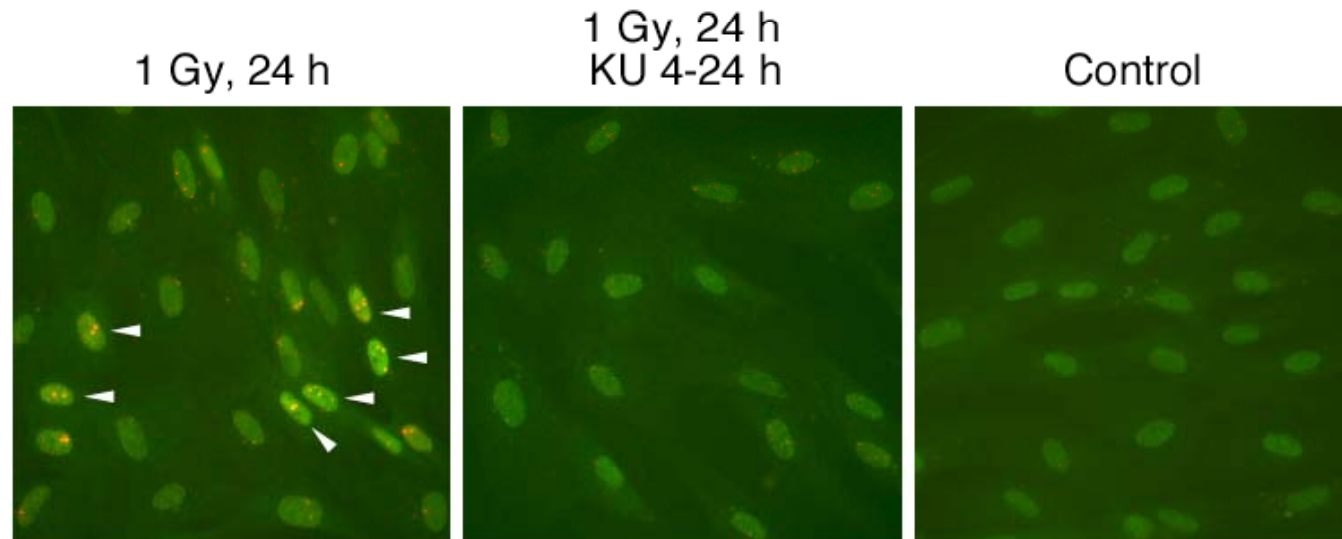
Treatment	Diameter of phosphorylated ATM focus (μ m)
1 Gy, 24 h	2.0 ± 0.8
1 Gy, 24 h KU 4-24 h	0.5 ± 0.2

Figure 5

(D)



(E)



Green : Phosphorylated p53 (Ser15)
Red : Phosphorylated ATM (Ser1981)

Table 1

Time after 1 Gy of X-rays	No. of cells analyzed	Phosphorylated ATM foci (+) (%)	Phosphorylated ATM large foci (+) ($\geq 1.6 \mu\text{m}$) (%)
C	189	18 (9.5)	12 (6.3)
1 h	204	204 (100)	0 (0)
2 h	198	198 (100)	1 (0.5)
4 h	179	179 (100)	6 (3.4)
8 h	181	181 (100)	24 (13.3)
12 h	144	125 (86.8)	25 (17.4)
24 h	152	97 (63.8)	34 (22.3)

Table 2

Cell cycle phase	Control			1 Gy, 24 h		
	Total (%)	% of cells with		Total (%)	% of cells with	
		Small foci (<1.6 μm)	Large foci ($\geq 1.6 \mu\text{m}$)		Small foci (<1.6 μm)	Large foci ($\geq 1.6 \mu\text{m}$)
G1	43.7	5.1	4.3	70.0	20.2	14.7
S	39.4	6.9	0.1	24.7	10.6	0.2
G2/M	16.9	1.6	0	5.3	1.3	0

Table 3

	Foci positive (%)	% of cells with	
		Small foci (<1.6 μm)	Large foci ($\geq 1.6 \mu\text{m}$)
RPA (+)			
WG1799 (NBS)			
Control	37.1	37.1	0
1 Gy, 24 h	83.6	83.6	0
HE49 (Normal)			
Control	18.5	18.1	0.4
1 Gy, 24 h	46.8	45.9	0.9
RPA (-)			
WG1799 (NBS)			
Control	37.3	35.9	1.4
1 Gy, 24 h	85.8	84.5	1.3
HE49 (Normal)			
Control	22.1	19.1	3.0
1 Gy, 24 h	62.0	40.4	21.6